Available online at www.sciencedirect.com
SCIENCE DIRECT®
International Journal of Heat and Mass Transfer 48 (2005) 183–190
International Journal of HEAT and MASS TRANSFER
www.elsevier.com/locate/ijhmt

Statistical optimization of a DC–RF hybrid plasma flow system for in-flight particle treatment

K. Kawajiri, K. Ramachandran, H. Nishiyama *

Electromagnetic Intelligent Fluids Laboratory, Intelligent Fluid Systems Division, Institute of Fluid Science, Tohoku University, 2-1-1 Katahira, Aoba-ku, Sendai 980-8577, Japan

Received 19 January 2004
Available online 22 October 2004

Abstract

There are many input parameters to control a DC–RF hybrid plasma flow system, such as total gas flow rate, central gas flow rate, swirl gas ratio, RF power and DC power. Furthermore, the interactive effects among these parameters should be considered. In the present study, statistical analysis using simple linear model is conducted to clarify the effects of the input parameters and their interactions on the outputs such as particle residence time and average temperature in a DC–RF hybrid plasma flow system. The thermofluid characteristics of a DC–RF hybrid plasma flow are compared with those of an RF plasma flow. It is shown that the plasma characteristics are changed drastically by adding even small DC power. Furthermore, controllability is also improved by optimizing the operating conditions of a DC–RF hybrid plasma flow system.

Keywords: DC–RF hybrid plasma flow; Thermofluid field; Particle; Statistical analysis; Interaction; Optimization

1. Introduction

A radio frequency (RF) plasma flow has been investigated intensively [1–9] for the material processing such as plasma spraying and fine particle treatment so far [10–17]. However, an RF plasma has some disadvantages of difficult generation and plasma instability. Then, a DC–RF hybrid plasma flow [18–20] has been expected to overcome such disadvantages of an RF plasma flow and to improve the plasma function. In a DC–RF hybrid plasma flow system, a direct current (DC) plasma jet is added as a supplement to an RF plasma flow. However, there is a strong interaction between an RF plasma flow and a DC plasma jet. Then, it is very important to understand the plasma characteristics in the controllable range of operating condition in details for material processing. Particularly, injected particle residence time and plasma temperature in plasma flow system are considered to be the most important factors for in-flight particle treatment to enhance heat transfer from plasma to particles and its efficiency.

There are many input parameters to control a DC–RF hybrid plasma flow system such as total gas flow rate, central gas flow rate, swirl gas ratio, RF power and DC power. And also, interactive effects among each

* Corresponding author. Tel./fax: +81 022 217 5260.
E-mail address: nishiyama@ifs.tohoku.ac.jp (H. Nishiyama).

0017-9310/$ - see front matter © 2004 Elsevier Ltd. All rights reserved.
doi:10.1016/j.ijheatmasstransfer.2004.07.037

Nomenclature

P_{DC}	DC power, kW	T_m	average temperature of plasma flow, K
P_{RF}	RF power, kW	t_r	particle residence time, s
Q_C	central gas flow rate, Sl/min	z	axial coordinate, mm
Q_{Sh}	sheath gas flow rate, Sl/min	e	contribution ratio of sum of neglected parameters, %
Q_{Sw}	swirl gas flow rate, Sl/min		
Q_T	total gas flow rate (= $Q_C + Q_{Sh}$), Sl/min	T	total contribution ratio of sum of every parameters, %
r	radial coordinate, mm		
R_{Sw}	swirl gas ratio (= Q_{Sw}/Q_{Sh}), %		

input parameter should be considered to analyze the complex causation. Taguchi method [21,22] is adopted to conduct the experiment effectively and to analyze results statistically [23,24]. In the present study, the contribution ratios of each input parameters to the output parameters such as particle residence time and average plasma temperature are obtained in their controllable range. Particle residence time and average plasma temperature are represented by regression equation for both an RF plasma flow and a DC–RF hybrid plasma flow. The statistically analyzed results of a DC–RF hybrid plasma flow are compared with those of an RF plasma flow. Finally, the operating conditions are statistically optimized from these obtained results.

2. Experimental procedures

2.1. Experimental setup and measuring methods

Fig. 1 shows the schematic illustration of the experimental apparatus. This system consists of RF plasma torch (5, 6 kW, 4 MHz), DC plasma torch (1, 2 kW), reaction chamber, powder feeder, gas supply control systems for an RF plasma torch and a DC plasma torch, monitoring system and vacuum system.

Fig. 2 shows the schematic illustration of a DC–RF hybrid plasma flow system with gas injections. This system consists of three-turn RF induction coils, DC electrodes which are installed at the top of an RF torch

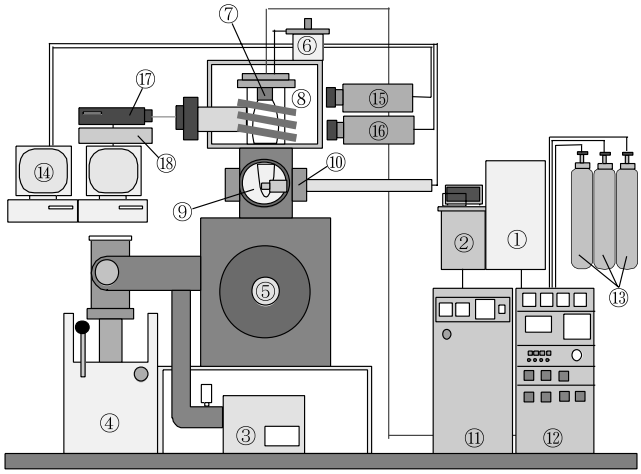

① Power supply for RF plasma torch
② Power supply for DC plasma torch
③ Rotary pump 1
④ Rotary pump 2
⑤ Reaction chamber
⑥ Powder feeder
⑦ DC plasma torch
⑧ RF plasma torch
⑨ Window
⑩ Measuring port
⑪ Control panel for DC plasma torch
⑫ Control panel for RF plasma torch
⑬ Compressed gas cylinder
⑭ Monitoring system
⑮ ICCD camera
⑯ Spectroscope
⑰ Nd : YAG Laser
⑱ Laser pulse synchronizer

Fig. 1. Schematic illustration of the experimental apparatus.

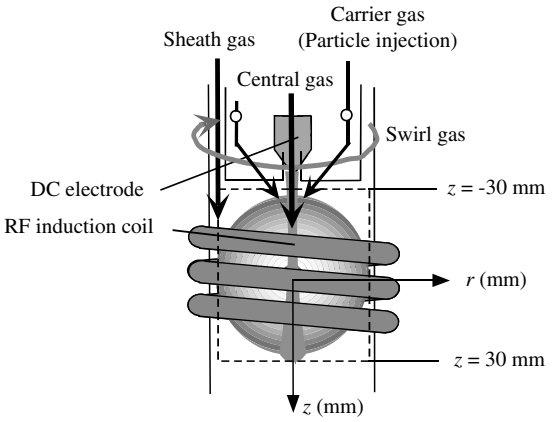

Fig. 2. Schematic illustration of a DC–RF hybrid plasma flow system with gas injections.

and water-cooled quartz tube of 44 mm inside diameter. There are mainly two kinds of gas injection modes to control a plasma flow. The sheath gas, which is the main gas to produce an RF plasma flow, is injected through the narrow space between the inner wall of the quartz tube of which diameter is 44 mm and the DC torch outside of which diameter is 40 mm, respectively. The central gas is injected through the central gas nozzle with diameter of 3 mm. The central gas nozzle is set at the center of the DC torch, and there are two carrier gas nozzles on 3.5 mm both sides of the central gas nozzle. The diameter of the carrier gas nozzle is 1.5 mm. The central gas is discharged to produce a DC plasma jet. The swirl gas is mixed with the sheath gas before the sheath gas is injected into the RF torch, and it gives the circumferential velocity to the sheath gas to stabilize a plasma flow and to protect the quartz tube thermally. The particles are injected diagonally from the two carrier gas nozzles into the plasma torch by the carrier gas of 0.3 Sl/min as shown in Fig. 2. The operating pressure in the plasma torch is changed from about 50 Torr to 80 Torr by changing the total gas flow rate from 10 Sl/min to 20 Sl/min.

The particle velocity in the RF induction coil region is measured with the particle image velocimetry (PIV) system. As the first output parameter of the DC–RF hybrid plasma flow system, particle residence time t_r (s) from $z = -30$ mm to $z = 30$ mm is obtained from particle velocity in the centerline region. In our PIV system, alumina particles of 10 μm is injected as a tracer. Nd: YAG laser, of which power, wave length and sheet thickness are 100 mJ, 532 nm and 2 mm, respectively is used. The laser pulse is emitted from the left side to the RF induction coil region and the flow image is captured in the front side of the window by CCD camera. The visualized results are obtained by averaging 20 images. The excitation temperature is measured at the four points ($z = -22.5$, -7.5, 7.5 and 22.5 mm) by the spectroscope in the central region. Boltzmann plot method is used to obtain the excitation temperature. The wave lengths of Ar I ($\lambda = 763.51$, 801.48, 811.53, 840.82, 912.30 nm) are adopted to obtain the excitation temperatures. Here, we assume that the plasma flow is optically thin in L.T.E. and then it has Boltzmann distribution. As the second output parameter, the average plasma temperature T_m (K) is obtained by averaging the temperatures at four points in the centerline region.

2.2. Experimental design

Statistical optimization is conducted according to a process as follows. At first, considerable input parameters and interactions are chosen to conduct experiments, and experimental conditions are determined according to an assignment of input parameters and interactions for an orthogonal array (OA) [21,22]. Secondly, *F*-ratio and contribution ratios of every input parameters and interactions are determined by analysis of variance (ANOVA) [21,22]. Parameters, of which *F*-ratio [22] is large and contribution ratio is small, are neglected in this process; where *F*-ratio is statistical value and it means a risk of assuming an input parameter as valid. Thirdly, a formula, which shows an interaction between every inputs and one output, is obtained from ANOVA. Finally, optimization is conducted to improve an output performance by controlling input parameters according to an obtained formula.

Table 1 shows the experimental conditions for an RF-ICP flow. For an RF-ICP flow, the following four parameters are chosen as input parameters in the statistical analysis independently, total gas flow rate (Q_T Sl/min), central gas flow rate (Q_C Sl/min), swirl gas flow

Table 1
Operating conditions for an RF plasma flow

Experimental number	Q_T [Sl/min]	Q_C [Sl/min]	R_{Sw} [%]	P_{RF} [kW]
1	10	3	20	5
2	10	3	20	6
3	10	3	80	5
4	10	3	80	6
5	10	6	20	5
6	10	6	20	6
7	10	6	80	5
8	10	6	80	6
9	20	3	20	5
10	20	3	20	6
11	20	3	80	5
12	20	3	80	6
13	20	6	20	5
14	20	6	20	6
15	20	6	80	5
16	20	6	80	6

Table 2
Operating conditions for a DC–RF plasma flow

Experimental number	Q_T [Sl/min]	Q_C [Sl/min]	R_{Sw} [%]	P_{RF} [kW]	P_{DC} [kW]
1	10	3	20	5	1
2	10	3	20	6	2
3	10	3	80	5	2
4	10	3	80	6	1
5	10	6	20	5	2
6	10	6	20	6	1
7	10	6	80	5	1
8	10	6	80	6	2
9	20	3	20	5	2
10	20	3	20	6	1
11	20	3	80	5	1
12	20	3	80	6	2
13	20	6	20	5	1
14	20	6	20	6	2
15	20	6	80	5	2
16	20	6	80	6	1

ratio (R_{Sw} %) which is defined as dividing the swirl gas flow rate by the sheath gas flow rate (Q_{Sw}/Q_{Sh}) and RF power (P_{RF} kW). In addition, the following six interactions of $Q_T * Q_C$, $Q_T * R_{Sw}$, $Q_T * P_{RF}$, $Q_C * R_{Sw}$, $Q_C * P_{RF}$ and $R_{Sw} * P_{RF}$ are considered in statistical analysis; where the asterisk shows an interaction between both side of it. Each input parameter and each interaction among these parameters are assigned for orthogonal array (OA_{16}) [21,22] and experimental conditions are determined as shown in Table 1.

Table 2 shows the experimental conditions for a DC–RF hybrid plasma flow. For a DC–RF hybrid plasma flow, an input parameter of DC power (P_{DC} kW) is newly added to four input parameters of an RF-ICP flow. Additionally, the following four interactions of $Q_T * P_{DC}$, $Q_C * P_{DC}$, $R_{Sw} * P_{DC}$ and $P_{RF} * P_{DC}$ are considered in addition to the six interaction of an RF-ICP flow.

3. Results and discussion

Table 3 shows the experimental results. The average plasma temperature in the centerline region of a DC–RF hybrid plasma flow is about twice that of an RF plasma flow. The following discussions are made to increase the particle residence time and the excitation temperature even for small input power of plasma torch. This is because the DC power and the RF power are somewhat small in our systems, and then the efficiency of the heat transfer from plasma to particles should be enhanced at first.

Table 4 shows the contribution ratios of input parameters. These values are determined by the analysis of variance (ANOVA) [21,22] which is calculated from

Table 3
Residence time and average temperature

	RF plasma flow		DC–RF hybrid plasma flow	
	t_r (s)	T_m (K)	t_r (s)	T_m (K)
1	0.00114	6273	0.00104	10,228
2	0.00123	5935	0.00115	11,537
3	0.00100	5883	0.00112	11,440
4	0.00105	5895	0.00097	10,921
5	0.00098	6953	0.00110	11,698
6	0.00107	7608	0.00081	11,661
7	0.00115	5801	0.00072	10,248
8	0.00135	5863	0.00093	13,339
9	0.00197	5880	0.00113	13,403
10	0.00147	5723	0.00108	13,432
11	0.00164	5829	0.00148	12,027
12	0.00156	5874	0.00260	15,289
13	0.00111	5689	0.00074	11,202
14	0.00135	5751	0.00126	13,758
15	0.00113	5785	0.00107	15,047
16	0.00131	5872	0.00104	12,324

the obtained experimental results in Table 3. In ANOVA, the input parameter's effect on the output is neglected when F-possibility, which shows a possibility that it happens accidentally, is more than 0.1 in this paper. Contribution ratios of neglected input parameters are included in an error's contribution ratio e in the table. Total contribution ratio T should be 100% as shown in the bottom line in the table.

3.1. Particle residence time

The contribution ratio of each input parameter to particle residence time t_r is shown in Table 4. In case of an RF plasma flow, the effect of the central gas flow rate on particle residence time 15.08 is smaller than that of the total gas flow rate 38.00, because the absolute momentum of the central gas is much smaller than the total gas flow rate. The interactive effects between the central gas and the total gas flow rate or the RF power are large. From the experimental results, the following equation is obtained to describe the particle residence time by regression analysis. The parameter's effects, of which contribution ratio is less than 5%, are neglected to simplify the equation.

$$t_r = 1.28 \times 10^{-3} + 3.23 \times 10^{-5}(Q_T - 15) - 6.28 \times 10^{-5}(Q_C - 4.5) - 1.56 \times 10^{-5}(Q_T - 15) \times (Q_C - 4.5) + 9.55 \times 10^{-5}(Q_C - 4.5)(P_{RF} - 5.5) \quad (1)$$

In case of a DC–RF hybrid plasma flow compared with the RF plasma flow, while the effect of the total gas flow rate on particle residence time of 14.50 is smaller, the

Table 4
Contribution ratios of input parameters

	RF plasma flow			DC–RF hybrid plasma flow	
	t_r (s)	T_m (K)		t_r (s)	T_m (K)
Q_T	38.00	22.70	Q_T	14.50	41.32
Q_C	15.08	–	Q_C	18.59	–
$Q_T * Q_C$	20.10	9.38	$Q_T * Q_C$	–	3.74
R_{Sw}	–	14.19	R_{Sw}	–	2.40
$Q_T * R_{Sw}$	–	20.81	$Q_T * R_{Sw}$	12.41	–
$Q_C * R_{Sw}$	–	8.66	$Q_C * R_{Sw}$	–	–
P_{RF}	–	–	$P_{RF} * P_{DC}$	–	–
$Q_T * P_{RF}$	–	–	P_{RF}	–	8.44
$Q_C * P_{RF}$	7.49	–	$Q_T * P_{RF}$	–	–
$R_{Sw} * P_{RF}$	–	–	$Q_C * P_{RF}$	–	–
e	19.32	24.26	$R_{Sw} * P_{DC}$	–	5.69
T	100.00	100.00	$R_{Sw} * P_{RF}$	–	–
			$Q_C * P_{DC}$	–	1.95
			$Q_T * P_{DC}$	–	2.20
			P_{DC}	13.57	31.55
			e	40.92	2.69
			T	100.00	100.00

effect of the central gas flow rate of 18.59 is larger. This comes from that the effect of the central gas flow rate is enhanced by a DC discharge. Then, particle residence time in a DC–RF hybrid plasma flow is approximated as follows.

$$t_r = 1.14 \times 10^{-3} + 3.19 \times 10^{-5}(Q_T - 15) - 1.2 \times 10^{-4}(Q_C - 4.5) + 5.6 \times 10^{-6}(Q_T - 15) \times (R_{Sw} - 50) + 3.08 \times 10^{-4}(P_{DC} - 1.5) \quad (2)$$

However, the error's contribution ratio in a DC–RF hybrid plasma flow is 40.92. Thus, the effects of the neglected parameters are relatively large.

Fig. 3 shows particle residence time in an RF plasma flow from Eq. (1); when RF power is fixed at 5 kW. Particle residence time in the centerline region is increased by increasing the total gas flow rate but decreasing the central gas flow rate. This is because that the particles injected in the centerline region are repulsed by the strong back flow due to the recirculating eddy in the coil upstream region. This recirculating eddy is produced by the existence of the anode and Lorentz force [1–3,14,18,20]. Boulos et al. predicted numerically in their work that an effect of the upstream recirculating eddy is enhanced by increasing total gas flow rate [1]. Then, particle residence time increases with increasing the total gas flow rate. Particles in the centerline region are transported by the central gas. Then, particle residence time increases with decreasing the central gas.

Fig. 4 shows Particle residence time in a DC–RF hybrid plasma flow from Eq. (2); when the swirl gas ratio and the DC power are fixed at 80% and 2 kW, respectively. The tendency of the effects of the total gas flow rate and the central gas flow rate on particle residence

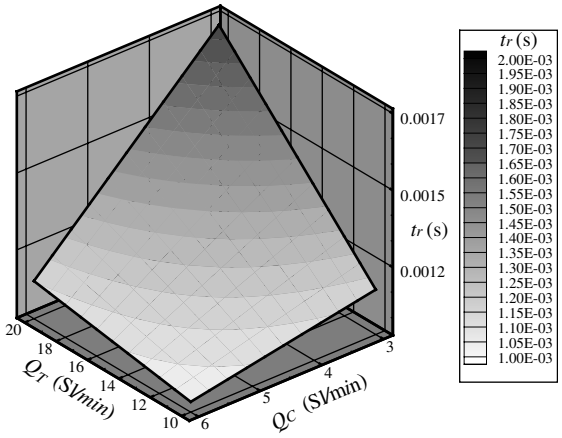

Fig. 3. Particle residence time in an RF plasma flow.

time is maintained in a DC–RF hybrid plasma flow too. However, compared with that in Fig. 4, each parameter in a DC–RF hybrid plasma flow can be controlled independently because of the weak interaction between the total gas flow rate and the central gas flow rate. We can understand that it is easier to control particle residence time in a DC–RF hybrid plasma flow than in an RF plasma flow because of the independency of each parameter's effect. However, it is not reasonable that particle residence time increases with increasing the DC power in Eq. (2), because the gas velocity in the central region is likely accelerated by adding DC discharge. The total momentum of the DC plasma jet is much smaller than that of the RF plasma flow, because the RF power is much higher than the DC power and the

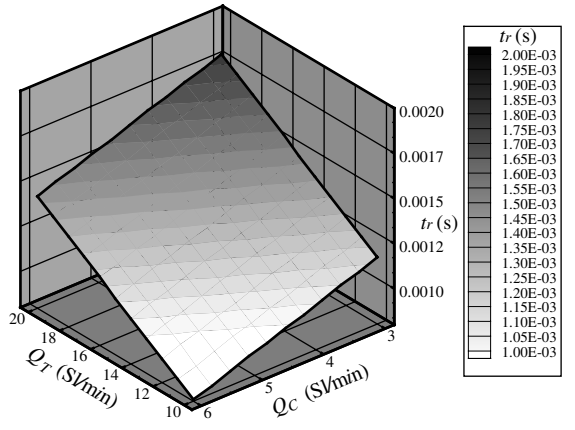

Fig. 4. Particle residence time in a DC–RF hybrid plasma flow.

central gas flow rate is considerably smaller than the total gas flow rate in the present study. Then, the effect of the DC plasma jet is not so strong itself in this system. However, the recirculating eddy in the core upstream region becomes stronger effectively with increasing the DC power because of the increase in the electrical conductivity especially in the RF coil region [18]. Consequently, the strong back flow due to the recirculating eddy overcomes the small and local acceleration effect by the DC plasma jet in the centerline region.

3.2. Average plasma temperature

Table 4 shows the contribution ratio of each input parameter on average plasma temperature. In case of an RF plasma flow, the effect of the DC power is neglected in the table. This reason comes from that the RF power level is small and its controllable range is also narrow in the present study. Then, it is understood that the effect of the power is relatively small within the present operating conditions compared with the effect of the other parameters. The most important parameters to control average plasma temperature are the total gas flow rate of 22.70 and the interaction between the total gas flow rate and the swirl gas ratio of 20.81. Therefore, the total gas flow rate and the swirl gas flow ratio should be controlled at first to increase average plasma temperature in an RF plasma flow. From the experimental results in Table 3, the following equation is obtained.

$$T_m = 6040 - 47.6(Q_T - 15) - 20.4(Q_T - 15) \times (Q_C - 4.5) - 6.27(R_{Sw} - 50) + 1.52(Q_T - 15) \times (R_{Sw} - 50) - 3.27(Q_C - 4.5)(R_{Sw} - 50) \quad (3)$$

However, the error's contribution ratio of 24.26 is relatively large. This means that, the effect of the neglected parameters is large.

On the other hand, in case of a DC–RF hybrid plasma flow, the contribution ratio of the each parameter is drastically changed from that in case of an RF plasma flow. This is caused by that radiation emitted from a DC–RF hybrid plasma flow is mainly from a DC plasma jet in the centerline region, because radiation intensity of a DC plasma jet is much stronger than that of an RF plasma flow. Then, the tendency of the contribution ratios is changed by adding DC discharge. The following equation is obtained from the experimental results in Table 3.

$$T_m = 12,300 + 193(Q_T - 15) + 859(P_{RF} - 5.5) + 23.8(R_{Sw} - 50)(P_{DC} - 1.5) + 1680(P_{DC} - 1.5) \quad (4)$$

Fig. 5 shows average plasma temperature in an RF plasma flow from Eq. (3); when the central gas flow rate is fixed at 6 Sl/min. The total gas flow rate should be decreased because the effective specific enthalpy of an RF plasma flow increases with decreasing the total gas flow rate at the fixed power. To increase average temperature in an RF plasma flow, the central gas flow rate should be increased more than 4.5 Sl/min with decreasing in the total gas flow rate and the swirl gas flow ratio should be less than 15 Sl/min and 50% respectively in Eq. (4).

Fig. 6 shows average plasma temperature in a DC–RF hybrid plasma flow from Eq. (4); when the RF power and the swirl gas ratio are fixed at 6 kW and 80%, respectively. As shown in this figure, on the contrary to an RF plasma flow, average plasma temperature increases with increasing the total gas flow rate. This is because gas velocity in the centerline region is decelerated by the strong back flow, which increases with increasing the total gas flow rate as described before. Then, heat transportation of a DC plasma jet in the axial direction is decreased by weak convection due to

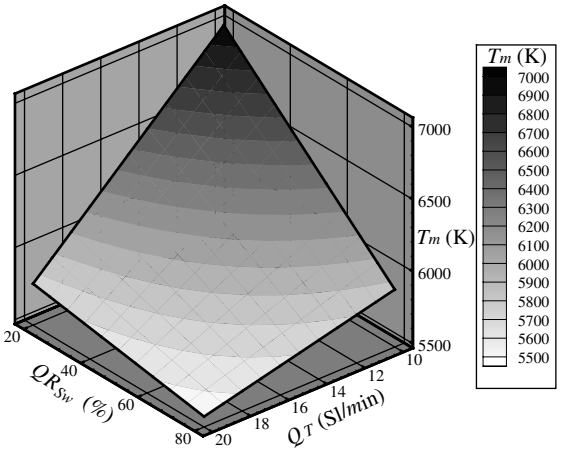

Fig. 5. Average temperature in an RF plasma flow.

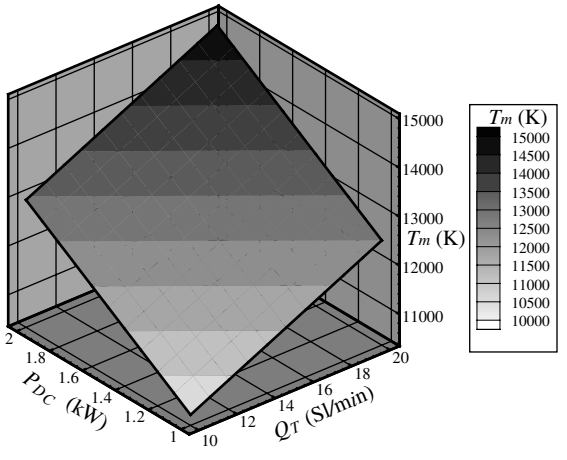

Fig. 6. Average temperature in a DC–RF hybrid plasma flow.

the back flow. Moreover, average plasma temperature increases with increasing the DC power because the effective specific enthalpy of a DC plasma jet is surely increased by increasing the DC power.

3.3. Optimization

Table 5 shows the optimum combination of input parameters to improve the outputs; where + and − indicate that the input parameter should be increased or decreased respectively to improve the each output. In the present operating conditions, the momentum of the DC plasma jet is much smaller than that of the RF plasma flow itself for the DC–RF hybrid plasma system, because the central gas flow rate and the DC power are small compared with the total gas flow rate and the RF power. However, the characteristics of the RF plasma flow are drastically changed by adding even small power of the DC plasma jet. This is because the interaction between the RF plasma flow and the DC plasma jet becomes much stronger, and then, such complex interaction affects unexpectedly this DC–RF hybrid plasma flow. In an RF plasma flow, the optimum control of input parameters to increase particle residence time is different from that to increase average plasma temperature. Therefore, the optimum control should be selected according to the most important output parameter in the applications. On the other hand, in a DC–RF hybrid plasma flow, the tendency is almost same for the each output. Therefore, particle residence time and average plasma temperature can be improved simultaneously by decreasing the central gas flow, but increasing totalgas flow rate, RF power, DC power and swirl gas flow.

Table 5
Optimized combination of input parameters to improve the outputs

	RF plasma flow		DC–RF hybrid plasma flow	
	Particle residence time	Average temperature	Particle residence time	Average temperature
Q_T	+	−	+	+
Q_C	−	+	−	−
R_{Sw}	−	−	+	+
P_{RF}	−	+	+	+
P_{DC}			+	+

4. Conclusions

Statistical optimization is conducted experimentally by using simple linear model of a DC–RF hybrid plasma flow system compared with an RF plasma flow system for in-flight particle treatment. The obtained results are as follows.

1. Plasma characteristics of an RF plasma flow and important parameters to control in-flight particle residence time and average plasma temperature are drastically changed by adding a DC plasma jet even with small power. Average plasma temperature in the central region is increased considerably by adding a DC plasma jet. The simple controllability for the outputs is improved to optimize the operating conditions in a DC–RF hybrid plasma flow.
2. Particle residence time and average plasma temperature for both an RF plasma flow and a DC–RF hybrid plasma flow are formularized by regression analysis in the controllable range of the present operating conditions.
3. Particle residence time and average plasma temperature are improved by decreasing central gas flow rate, but by increasing total gas flow rate, swirl gas ratio, RF power and DC power in a DC–RF hybrid plasma flow.

Acknowledgments

We would like to give our sincere thanks to senior technician Mr. K. Katagiri in our laboratory, and also to Mr. T. Watanabe and Mr. N. Ito in the institute workshop. This research was partially supported by a grant-in-aid for Scientific Research (B) from the Japan Society for Promotion of Science (2001–2003) and a 21st Century COE Program Grant of the International COE of Flow Dynamics from the Ministry of Education, Culture, Sports, Science and Technology.

References

[1] M.I. Boulos, IEEE Trans. Plasma Sci. 4 (1976) 28–39.
[2] J. Mostaghimi, M.I. Boulos, J. Appl. Phys. 68 (6) (1990) 2643–2648.
[3] Z. Njah, J. Mostaghimi, M.I. Boulos, Int. J. Heat Mass Transfer 36 (16) (1993) 3909–3919.
[4] M. Rahmane, G. Soucy, M.I. Boulos, Int. J. Heat Mass Transfer 37 (14) (1994) 2035–2046.
[5] S. Xue, P. Proulx, M.I. Boulos, Plasma Chem. Plasma Process. 23 (2) (2003) 245–263.
[6] D.T. Or, N.S. Subramanian, J.V.R. Heberlein, E. Pfender, IEEE Trans. Plasma Sci. 25 (5) (1997) 1034–1041.
[7] A. Gutsol, J. Larjo, R. Hernberg, Plasma Chem. Plasma Process. 22 (3) (2002) 351–369.
[8] P. Proulx, J. Mostaghimi, M.I. Boulos, Int. J. Heat Mass Transfer 34 (10) (1991) 2571–2579.
[9] T. Uesugi, O. Nakamura, T. Yoshida, K. Akashi, J. Appl. Phys. 64 (8) (1988) 3874–3879.
[10] T. Yoshida, K. Akashi, J. Appl. Phys. 48 (6) (1977) 2252–2260.
[11] P. Proulx, J. Mostaghimi, M.I. Boulos, Int. J. Heat Mass Transfer 28 (7) (1985) 1327–1336.
[12] P. Buchner, H. Ferfers, H. Schubert, J. Uhlenbusch, Plasma Sources Sci. Technol. 6 (1997) 450–459.
[13] J.H. Park, S.H. Hong, IEEE Trans. Plasma Sci. 23 (4) (1995) 532–537.
[14] M. Shigeta, T. Sato, H. Nishiyama, Int. J. Heat Mass Transfer 47 (2004) 707–716.
[15] Y.K. Chae, J. Moshtaghimi, T. Yoshida, Sci. Technol. Adv. Mater. 1 (2000) 147–156.
[16] M. Suzuki, M. Kagawa, Y. Syono, T. Hirai, J. Mater. Sci. 27 (1992) 679–684.
[17] N. Yamaguchi, T. Hattori, K. Terashima, T. Yoshida, Thin Solid Films 316 (1998) 185–188.
[18] T. Yoshida, T. Tani, H. Nishimura, K. Akashi, J. Appl. Phys. 54 (1983) 640–646.
[19] R. Shimpo, Y. Uehara, T. Yoshida, in: Proc. 14th Int. Symp. Plasma Chemistry, vol. 4, 1999, p. 2115.
[20] K. Kawajiri, T. Sato, H. Nishiyama, Surf. Coat. Technol. 171 (2003) 134–139.
[21] G. TaguchiSystems of Experimental Design, vols. 1 and 2, Japanese Standards Association, 1976, p. 1977.
[22] N. Logothetis, H.P. Wynn, Quality Through Design, Clarendon Press, Oxford, 1994.
[23] J.R. Mawdsley, Y.J. Su, K.T. Faber, T.F. Bernecki, Mater. Sci. Eng. A 308 (2001) 189–199.
[24] P. Saravanan, V. Selvarajan, S.V. Joshi, G. Sundararajan, J. Appl. Phys. D 34 (2001) 131–140.

Kohtaro Kawajiri is a Doctorial Candidate at the Graduate School of Engineering, Tohoku University, Japan. He obtained his Bachelors Degree in Mechanical Engineering from the Tohoku University in 2000 and his Master Degree in Mechanical Engineering from the Tohoku University in 2002.

Kandasamy Ramachandran is a Visiting Scientist at the Institute for Materials and Processes in Energy and System, Julich, Germany. He obtained his Bachelors Degree in Physics from the Bharathiar University, India, in 1989; Masters Degree in Physics from the Bharathiar University in 1991; Masters Degree in Plasma Physics from the Bharathiar University in 1992 and Ph.D. in Plasma Physics from the Bharathiar University in 1998. He was a Postdoctoral Research Fellow at the Bharathiar University in 1998. Lecturer at the PSG College of Technology, India, in 1999; Science and Technology Agency Fellow at the National Institute of Advanced Industrial Science and Technology, Japan, in 1999; Postdoctoral Research Fellow at the Tohoku University, Japan, in 2001; Research Associate at the Tohoku University in 2002, and is a Visiting Scientist at Forschungszentrum Julich GmbH, Germany in 2004.

Hideya Nishiyama is a Professor and the University Councillor at the Institute of Fluid Science, Tohoku University, Japan. He obtained his Bachelors Degree of Mechanical Engineering from Tohoku University, Japan, in 1977 and his Masters Degree in 1979 and further his Ph.D. in Mechanical Engineering from Tohoku University in 1982. He was a Research Associate at Mining College, Akita University, Japan, in 1982; worked as a Lecturer at Mining College in 1985; Associate Professor at Mining College in 1988; Associate Professor at the Institute of High Speed Mechanics, Tohoku University, Japan, in 1989. He was a Visiting Researcher at the Von Karman Institute for Fluid Dynamics, Belgium, in 1990; Professor at the Institute of Fluid Science, Tohoku University in 1997; and is the University Councillor, Tohoku University, Japan, in 2004. He has been awarded the Excellent Prize (Institute of Theoretical and Applied Mechanics, Siberian Branch of Russian Academy of Sciences), the JSME, Best Paper Award and the JSMF, Best Paper Prize.